Journal of the Egyptian Mathematical Society (2016) **24**, 458–470

Egyptian Mathematical Society

Journal of the Egyptian Mathematical Society

www.etms-eg.org
www.elsevier.com/locate/joems

Original Article

Finite element analysis of heat and mass transfer by MHD mixed convection stagnation-point flow of a non-Newtonian power-law nanofluid towards a stretching surface with radiation

Macha Madhu*, **Naikoti Kishan**

Department of Mathematics, Osmania University, Hyderabad, Telangana 500007, India

Received 6 August 2014; revised 24 May 2015; accepted 23 June 2015
Available online 26 September 2015

Keywords

Non-Newtonian;
Nanofluid;
Stagnation-point flow;
Brownian motion;
Power-law index;
Thermal radiation

Abstract Magnetohydrodynamic mixed convection boundary layer flow of heat and mass transfer stagnation-point flow of a non-Newtonian power-law nanofluid towards a stretching surface in the presence of thermal radiation is investigated numerically. The non-Newtonian nanofluid model incorporates the effects of Brownian motion and thermophoresis. The basic transport equations are made dimensionless first and the coupled non linear differential equations are solved by finite element method. The numerical calculations for velocity, temperature and concentration profiles for different values of the physical parameters presented graphically and discussed. As well as for skin friction coefficient, local Nusselt and Sherwood numbers exhibited and examined.

2010 Mathematics Subject Classification: 76A05; 80A20; 80M10

1. Introduction

In recent years, the study of flow and heat transfer of non-Newtonian fluids has received considerable attention because of its wide use of these fluids in food engineering, petroleum production, power engineering and in many industries such as polymer melt and polymer solutions used in the plastic processing industries. Over recent years, applications of non-Newtonian fluids in many industrial processes have been interesting. Many particulate slurries, multiphase mixers, pharmaceutical formulation, cosmetics and toiletries, paints, biological fluids, and food items are examples of non-Newtonian fluids. Many of

* Corresponding author. Tel.: +91- 9248358378.
E-mail addresses: madhumaccha@gmail.com (M. Madhu), kishan_n@rediffmail.com (N. Kishan).
Peer review under responsibility of Egyptian Mathematical Society.

ELSEVIER Production and hosting by Elsevier

http://dx.doi.org/10.1016/j.joems.2015.06.001

Nomenclature

C	Nanoparticle volume fraction
C_{f_x}	Skin friction coefficient
D_B	Brownian diffusion
D_T	Thermophoretic diffusion coefficient
f	Dimensionless stream function
g	Acceleration due to gravity
k	Thermal conductivity
K	Consistency coefficient of the fluid
Le	Generalized Lewis number
M	Magnetic parameter
N	Concentration to thermal buoyancy ratio
n	Power-law rheological index
Nb	Generalized Brownian motion parameter
Nt	Generalized thermophoresis parameter
Nu_x	Local Nusselt number
Pr_x	Generalized Prandtl number
R_d	Radiation parameter
Re	Reynolds number
Re_x	Local Reynolds number
Sh_x	Local Sherwood number
T	Fluid temperature
u, v	Velocity components
x, y	Cartesian coordinates
α_m	Thermal diffusivity
Λ	dimensionless mixed convection parameter
υ	Kinematic viscosity of the fluid
ρ_f	Fluid density
ρ_p	Nanoparticle mass density
τ	Ratio between the effective heat capacity of the nanoparticle material and heat capacity of the fluid
θ	Dimensionless temperature
ϕ	Dimensionless nanoparticle volume fraction
ψ	Stream function
η	Similarity independent variable
w	Conditions at the wall
∞	Ambient condition
$'$	Prime denotes the derivative with respect to η

the non-Newtonian fluids encountered in chemical engineering processes are known to follow the empirical Ostwaldde Waele power-law model. The concept of boundary layer was applied to power-law fluids by Schowalter [1]. Acrivos [2] investigated the boundary-layer flows for such fluids in 1960, since then a large number of related studies have been conducted because of their importance and presence of such fluids in chemicals, polymers, molten plastics and others. Most of the previous studies of natural convection associated with clear fluid media have considered Newtonian fluids, which received a great attention among the thermofluid community. Few theoretical studies have investigated the shear rate effect of non-Newtonian fluids on convective flow patterns and heat transfer rate, despite their importance and presence in many industrial applications such as paper making, oil drilling, slurry transporting, food processing, and polymer engineering.

The theory of non-Newtonian fluids offers mathematicians, engineers and numerical specialists varied challenges in developing analytical and numerical solutions for the highly non-linear governing equations. However, due to the practical significance of these non-Newtonian fluids, many authors have presented various non-Newtonian fluid models like Elbashbeshy et al. [3], Nadeem et al. [4], Nadeem et al. [5], Nadeem et al. [6], Nadeem and Akbar [7], Nadeem and Ali [8], Buongiorno [9], Lukaszewics [10]. Many interesting applications of non-Newtonian power-law fluids were presented by Shenoy [11]. Details of the behavior of non-Newtonian fluids for both steady and unsteady flow situations, along with mathematical models are studied by Astarita and Marrucci [12], Bhome [13], Kishan [14] and Kavitha [15].

Nanotechnology has immense applications in industry since materials with sizes of nanometers exhibit unique physical and chemical properties. Fluids with nano-scaledparticles interaction are called as nanofluid. It represents the most relevant technological cutting edge currently being explored. Nanofluid heat transfer is an innovative technology which can be used to enhance heat transfer. Nanofluid is a suspension of solid nanoparticles (1–100 nm diameters) in conventional liquids like water, oil and ethylene glycol. Depending on shape, size, and thermal properties of the solid nanoparticles, the thermal conductivity can be increased by about 40% with low concentration (1–5% by volume) of solid nanoparticles in the mixture. The nano particles used in nanofluid are normally composed of metals, oxides, carbides or carbon nanotubes. Water, ethylene glycol and oil are common examples of base fluids. Nanofluid have their major applications in heat transfer, including microelectronics, fuel cells, pharmaceutical processes and hybrid-powered engines, domestic refrigerator, chiller, nuclear reactor coolant, grinding, space technology and in boiler flue gas temperature reduction. They demonstrate enhanced thermal conductivity and convective heat transfer coefficient counterbalanced to the base fluid. Nanofluid has been the core of attention of many researchers for new production of heat transfer fluids in heat exchangers, plants and automotive cooling significations, due to their enormous thermal characteristics Nadeem et al. [16].

The nanofluid is stable, it introduce very little pressure drop, and it can pass through nanochannels (for more instance see Zhou [17]). The word nanofluid was coined by Choi [18]. Xuan and Li [19] pointed out that at higher nanoparticle volume fractions, the viscosity increases sharply, which suppresses heat transfer enhancement in the nanofluid. Therefore, it is important to carefully select the proper nanoparticle volume fraction to achieve heat transfer enhancement. Buongiorno [9] noted that the nanoparticles absolute velocity can be viewed as the sum of the base fluid velocity and a relative velocity (that he called the slip velocity). He considered in turn seven slip mechanisms: inertia, Brownian diffusion, thermophoresis, diffusiophoresis, Magnus effect, fluid drainage, and gravity settling.

Forced convective heat transfer can be enhanced effectively by using nanofluids, a type of fluid adding different suspending nanoparticles into the conventional base liquid (Pak and Cho [20], Wen and Ding [21], Ding et al. [22]). However, the characteristics of nanofluids and the mechanism of the enhancement of the forced convective heat transfer of nanofluids are still not clear. Recently nanofluids have attracted much attention since anomalously large enhancements in effective thermal conductivities were reported over a decade ago (Choi [18], Masuda [23], Keblinski et al. [24]). Subsequent studies by various groups have reported that nanofluids also have other desirable properties and behaviors such as enhanced wetting and spreading (Wasan et al. [25], Chengara et al. [26]), as well as increased critical heat

fluxes under boiling condition (You et al. [27]). Sheikholeslami et.al [28] studied the effects of heat transfer in flow of nanofluids over a permeable stretching wall in a porous medium.

Boundary layer flow and heat transfer over a continuously stretched surface has received considerable attention in recent years. This is because of the various possible engineering and metallurgical applications such as hot rolling, metal and plastic extrusion, wire drawing, glass fiber production, continuous casting, crystal growing, and paper production. Crane [29] was the first to investigate the boundary layer flow caused by a stretching sheet moving with linearly varying velocity from a fixed point whilst the heat transfer aspect of the problem was investigated by Carragher and Crane [30] under the conditions that the temperature difference between the surface and the ambient fluid was proportional to the power of the distance from a fixed point.

A recent development in fluid mechanics has been the study of nanofluids which possess superior thermal conductivity properties and enhance heat transfer in fluids. Thus the behavior of non-Newtonian nanofluids could be useful in evaluating the possibility of heat transfer enhancement in various processes of these industries. Several investigators have studied non-Newtonian nanofluid transport in various geometries under various boundary conditions in porous or non-porous media. Ellahi et al. [31] have elaborated that non-Newtonian nanofluids have potential roles in physiological transport as biological solutions and also in polymer melts, paints, etc. Non-Newtonian nanofluid is important in many industrial and technological applications such as biological solutions, melts of polymers, paint, tars and glues (Ellahi et al. [31–33]). Because of this, research works on non-Newtonian fluids have recently become very important. Transport phenomena associated with magnetohydrodynamics arise in physics, geophysics, astrophysics and many branches of chemical engineering which includes crystal magnetic damping control, hydromagnetic chromatography; conducting flow in trickle-bed reactors and enhanced magnetic filtration control (Prasad et al. [34]).

The objective of the present study is to investigate the effects of MHD and thermal radiation on heat and mass transfer by mixed convection boundary layer stagnation point flow of non-Newtonian power law fluid towards a stretching surface with a nanofluid. The effect of Brownian motion, thermophoresis are included for the nanofluid. Numerical solutions of the boundary layer equations are obtained and a discussion is provided for several values of the nanofluid parameters governing the problem. The dimensionless profiles of velocity, temperature and nano particle volume fraction as well as the skin friction coefficient, local Nusselt number and Sherwood number for the different flow parameters have been discussed.

2. Mathematical formulation

Consider steady, laminar, heat and mass transfer by mixed convection, boundary layer stagnation-point flow of an electrically-conducting, optically dense and non-Newtonian power-law fluid obeying the Ostwald-de Waele model (see, Metzner (1965)) past a heated or cooled stretching vertical surface in the presence of thermal radiation. It is assumed that the stretching velocity is given by $u_w(x) = cx$, and the velocity distribution in frictionless potential flow in the neighborhood of the stagnation point at $x = y = 0$ is given by $U(x) = ax$. We assumed that the uniform wall temperature T_w and nanoparticles volume fraction C_w are higher than that of their full stream values T_∞, C_∞. A uniform magnetic field is applied in the y-direction normal to the flow direction. The magnetic Reynolds number is assumed to be small so that the induced magnetic field is neglected. In addition, the Hall effect and the electric field are assumed negligible. The small magnetic Reynolds number assumption uncouples the Navier–Stokes equations from Maxwells equations. All physical properties are assumed constant except the density in the buoyancy force term. By invoking all of the boundary layer, Boussineq and Rosseland diffusion approximations, the governing equations for this investigation can be written as;

$$\frac{\partial u}{\partial x} + \frac{\partial v}{\partial y} = 0, \tag{1}$$

$$u\frac{\partial u}{\partial x} + v\frac{\partial u}{\partial y} = U\frac{dU}{dx} + \frac{1}{\rho}\frac{\partial \tau_{xy}}{\partial y} + g\beta(T - T_\infty) + g\beta^*(C - C_\infty) - \frac{\sigma B_0^2}{\rho}(u - U), \tag{2}$$

$$u\frac{\partial T}{\partial x} + v\frac{\partial T}{\partial y} = \alpha_m\frac{\partial^2 T}{\partial y^2} + \tau\left[D_B\frac{\partial C}{\partial y}\frac{\partial T}{\partial y} + \frac{D_T}{T_\infty}\left(\frac{\partial T}{\partial y}\right)^2\right] - \frac{1}{\rho C_p}\frac{\partial q_r}{\partial y}, \tag{3}$$

$$u\frac{\partial C}{\partial x} + v\frac{\partial C}{\partial y} = D_B\frac{\partial^2 C}{\partial y^2} + \frac{D_T}{T_\infty}\frac{\partial^2 T}{\partial y^2}. \tag{4}$$

The associated boundary conditions are

$$u = u_w(x) = cx, \quad v = 0, \quad T = T_w, \quad C = C_w \quad at \quad y = 0, \tag{5a}$$

$$u = U(x) = ax, \quad v = -ay, \quad T = T_\infty, \quad C = C_\infty \quad at \quad y \to \infty. \tag{5b}$$

u, v, T and C are the $x-$ and y components of velocity, temperature and nanoparticle volume fraction, respectively. g, ρ, α_m, D_B, D_T, B_0, β and β^* are the gravitational acceleration, fluid density, thermal diffusivity, Brownian diffusion coefficient, thermophoretic diffusion coefficient, magnetic field, coefficient of thermal expansion, and coefficient of concentration of expansion, respectively. we have $\frac{\partial u}{\partial y} > 0$ when $a/c > 1$ (the ratio of free stream velocity and stretching velocity) which gives the shear stress as:

$$\tau_{xy} = K\frac{\partial}{\partial y}\left(\frac{\partial u}{\partial y}\right)^n. \tag{6}$$

Where K is the consistency coefficient and n is the power-law index. It needs to be mentioned that for the non-Newtonian power law model, the case of $n < 1$ is associated with shear-thinning fluids (pseudoplastic fluids), $n = 1$ corresponds to Newtonian fluids and $n > 1$ applies to the case of shear-thickening (dilatant).

Using the Rosseland approximation for radiation, the radiative heat flux is simplified as:

$$q_r = -\frac{4\sigma_1}{3\chi}\frac{\partial T^4}{\partial y}, \tag{7}$$

where σ_1 and χ are the Stefan–Boltzmann constant and the mean absorption coefficient, respectively. We assume that the

temperature differences within the flow, such as the term T^4, may be expressed as a linear function of temperature. Hence, expanding T^4 in a Taylor series about a free stream temperature T_∞ and neglecting higher-order terms, we get:

$$T^4 = 4T_\infty^4 T - 3T_\infty^4. \tag{8}$$

Using (7) and (8) in the last term of Eq. (3), we obtain

$$\frac{\partial q_r}{\partial y} = -\frac{16\sigma_1 T_\infty^3}{3\chi}\frac{\partial^2 T}{\partial y^2}. \tag{9}$$

In order to reduce the governing equations into a system of ordinary differential equations, the following dimensionless parameters are introduced

$$\psi = \left(\frac{K/\rho}{c^{1-2n}}\right)^{\frac{1}{n+1}} x^{\frac{2n}{n+1}} f(\eta),\ \theta = \frac{T-T_\infty}{T_w-T_\infty},\ \phi = \frac{C-C_\infty}{C_w-C_\infty},$$
$$\eta = y\left(\frac{c^{2-n}}{K/\rho}\right)^{\frac{1}{n+1}} x^{\frac{1-n}{1+n}}. \tag{10}$$

It is worth mentioning that the continuity equation is identically satisfied from our choice of the stream function with $u = \frac{\partial \psi}{\partial y}$ and $v = -\frac{\partial \psi}{\partial x}$. Substituting the dimensionless parameters into Eqs. (2)–(4) gives

$$n(f'')^{(n-1)} f''' + \left(\frac{2n}{n+1}\right) f f'' - f'^2 - M f' + M\frac{a}{c} + \frac{a^2}{c^2} + \Lambda(\theta + N\phi) = 0, \tag{11}$$

$$\frac{1}{Pr}\left(1 + \frac{4R_d}{3}\right)\theta'' + \left(\frac{2n}{n+1}\right) f\theta' + Nb\theta'\phi' + Nt\theta'^2 = 0, \tag{12}$$

$$\phi'' + \left(\frac{2n}{n+1}\right) Le f\phi' + \frac{Nt}{Nb}\theta'' = 0. \tag{13}$$

The transformed boundary conditions are

$$f(0) = 0,\ \ f'(0) = 1,\ \ \theta(0) = 1,\ \ \phi(0) = 1, \tag{14a}$$

$$f'(\infty) \to a/c,\ \ \theta(\infty) \to 0,\ \ \phi(\infty) \to 0. \tag{14b}$$

The eight parameters appearing in Eqs. (11)–(13) are defined as follows

$$M = \frac{\sigma B_0^2}{\rho c},\ \Lambda = \frac{g\beta(T_w - T_\infty)x^3/\upsilon^2}{u_w^2 x^2/\upsilon^2},\ N = \frac{g\beta^*(C_w - C_\infty)}{g\beta(T_w - T_\infty)},$$
$$Pr = \frac{\upsilon}{\alpha_m}\left(c^2 Re_x\right)^{\frac{n-1}{n+1}},\ R_d = \frac{4\sigma_1 T_\infty^3}{3k\chi},$$
$$Nb = \frac{\tau D_B(C_w - C_\infty)}{\upsilon}\left(c^2 Re_x\right)^{\frac{1-n}{1+n}},$$
$$Nt = \frac{\tau D_T(T_w - T_\infty)}{T_\infty \upsilon}\left(c^2 Re_x\right)^{\frac{1-n}{1+n}},\ Le = \frac{\upsilon}{D_B}\left(c^2 Re_x\right)^{\frac{n-1}{n+1}}. \tag{15}$$

where $Re_x = \frac{u_w x}{\upsilon}$ is the local Reynolds number based on the stretching velocity $u_w(x)$ and k is the thermal conductivity. It should be noted that $\Lambda > 0$ corresponds to an assisting flow (heated plate), $\Lambda < 0$ corresponds to an opposing flow (cooled plate) and $\Lambda = 0$ yields forced convection flow.

The skin-friction coefficient C_{f_x} at the wall is given by:

$$C_{f_x} = 2\left[f''(0)\right]^n \left(\frac{(cx)^{2-n}x^n}{K/\rho}\right)^{-1/(1+n)}, \tag{16}$$

the local Nusselt number Nu_x is given by:

$$Nu_x = -K\left(\frac{u_w^{2-n}}{K/\rho}\right)^{1/n+1}\left(1 + \frac{4R_d}{3}\right)\theta'(0), \tag{17}$$

and the local Sherwood number Sh_x is given by:

$$Sh_x = -D\left(\frac{u_w^{2-n}}{K/\rho}\right)^{1/n+1}\phi'(0). \tag{18}$$

3. Method of solution

3.1. Finite element method

The finite element method is a powerful technique for solving ordinary or partial differential equations. The basic concept of FEM is that the whole domain is divided into smaller elements of finite dimensions called Finite Elements. This method is the most versatile numerical technique in engineering analysis and has been employed to study diverse problems in heat transfer, fluid mechanics, rigid body dynamics, solid mechanics, chemical processing, electrical systems, acoustics and many other fields. The steps involved in the finite element analysis are as follows:

- Discretization of the domain into elements
- Derivation of element equations
- Assembly of Element Equations
- Imposition of boundary conditions
- Solution of assembled equations

To solve the system of simultaneous nonlinear differential equations (11)–(13), with the boundary conditions (14a) and (14b), we assume

$$f' = h, \tag{19}$$

the system of equations (11)–(13) then reduced to

$$n(h')^{(n-1)}h'' + \left(\frac{2n}{n+1}\right) f h' - h^2 - Mh + M\frac{a}{c} + \frac{a^2}{c^2} + \Lambda(\theta + N\phi) = 0, \tag{20}$$

$$\frac{1}{Pr}\left(1 + \frac{4R_d}{3}\right)\theta'' + \left(\frac{2n}{n+1}\right) f\theta' + Nb\theta'\phi' + Nt\theta'^2 = 0, \tag{21}$$

$$\phi'' + \left(\frac{2n}{n+1}\right) Le f\phi' + \frac{Nt}{Nb}\theta'' = 0, \tag{22}$$

and the corresponding boundary conditions now become

$$f(0) = 0,\ \ h(0) = 1,\ \ \theta(0) = 1,\ \ \phi(0) = 1, \tag{23a}$$

$$h(\infty) \to a/c,\ \ \theta(\infty) \to 0,\ \ \phi(\infty) \to 0. \tag{23b}$$

For computational purposes, the ∞ has been shifted to $\eta = 12$, without any loss of generality. The domain is divided into a set of 100 line elements, each element having two nodes.

Table 1 Comparison of $f''(0)$ for various values of M at $n = 1$, between analytical solutions obtained by homotopy analysis method and Finite Element Method in the present work in the absence of heat and mass transfer.

M	Mahapatra [35] Analytical results	Present results
0.0	2.0175	2.01753
0.5	2.1363	2.136374
1.0	2.2491	2.249134
1.5	2.3567	2.356684
2.0	2.4597	2.459658
3.0	2.6540	2.65378
5.0	3.0058	3.00392

Table 2 Computations of the Nusselt number, skin friction coefficient and the Sherwood number for various values of n and M.

n	M	$f''(0)$	$-(1+\frac{4R_d}{3})\theta'(0)$	$-\phi'(0)$
0.6	0	3.6758	2.1486	2.5703
	2	3.4341	2.1039	2.5378
	5	3.3008	2.0674	2.5167
1.0	0	2.4841	2.417	2.8058
	2	2.3783	2.3856	2.7928
	5	2.3458	2.3511	2.7822
1.6	0	1.5779	2.5715	2.9596
	2	1.5685	2.5454	2.9584
	5	1.5042	2.5239	2.9573

3.2. Variational formulation

The variational form associated with Eqs. (19)–(22) over a typical linear element (η_e, η_{e+1}) is given by

$$\int_{\eta_e}^{\eta_{e+1}} w_1\{f' - h\}\,\mathrm{d}\eta = 0, \tag{24}$$

$$\int_{\eta_e}^{\eta_{e+1}} w_2\left\{n(h')^{(n-1)}h'' + \left(\frac{2n}{n+1}\right)fh' - h^2 - Mh + M\frac{a}{c} + \frac{a^2}{c^2} + \Lambda(\theta + N\phi)\right\}\mathrm{d}\eta = 0, \tag{25}$$

$$\int_{\eta_e}^{\eta_{e+1}} w_3\left\{\frac{1}{Pr}\left(1+\frac{4R_d}{3}\right)\theta'' + \left(\frac{2n}{n+1}\right)f\theta' + Nb\theta'\phi' + Nt\theta'^2\right\}\mathrm{d}\eta = 0, \tag{26}$$

$$\int_{\eta_e}^{\eta_{e+1}} w_4\left\{\phi'' + \left(\frac{2n}{n+1}\right)Lef\phi' + \frac{Nt}{Nb}\theta''\right\}\mathrm{d}\eta = 0, \tag{27}$$

where w_1, w_2, w_3 and w_4 are weight functions and may be viewed as the variation in f, g, θ and ϕ respectively.

3.3. Finite element formulation

The finite element model from Eqs. (24)–(27) by substituting finite element approximations of the form

$$f = \sum_{j=1}^{2} f_j\psi_j,\ h = \sum_{j=1}^{2} h_j\psi_j,\ \theta = \sum_{j=1}^{2}\theta_j\psi_j,\ \phi = \sum_{j=1}^{2}\phi_j\psi_j, \tag{28}$$

with $w_1 = w_2 = w_3 = w_4 = \psi_i,\ (i = 1, 2)$,

Table 3 Computations of the Nusselt number, skin friction coefficient and the Sherwood number for various values of n and Nt.

n	Nt	$f''(0)$	$-(1+\frac{4R_d}{3})\theta'(0)$	$-\phi'(0)$
0.6	0.1	3.4350	2.1045	2.5381
	0.4	3.4652	2.0815	2.4863
	0.7	3.4933	2.0591	2.4399
1.0	0.1	2.3783	2.3856	2.7928
	0.4	2.3957	2.3594	2.7357
	0.7	2.4142	2.3332	2.6843
1.6	0.1	1.4992	2.5811	2.9845
	0.4	1.5387	2.5511	2.8973
	0.7	1.5408	2.5217	2.8453

where ψ_i are the shape functions for a two-nodded linear element (η_e, η_{e+1}) and are taken as

$$\psi_1^{(e)} = \frac{\eta_{e+1} - \eta}{\eta_{e+1} - \eta_e},\ \psi_2^{(e)} = \frac{\eta - \eta_e}{\eta_{e+1} - \eta_e},\ \eta_e \le \eta \le \eta_{e+1}. \tag{29}$$

The finite element model of the equations thus formed is given by:

$$\begin{bmatrix}[K^{11}] & [K^{12}] & [K^{13}] & [K^{14}]\\ [K^{21}] & [K^{22}] & [K^{23}] & [K^{24}]\\ [K^{31}] & [K^{32}] & [K^{33}] & [K^{34}]\\ [K^{41}] & [K^{42}] & [K^{43}] & [K^{44}]\end{bmatrix}\begin{bmatrix}\{f\}\\ \{h\}\\ \{\theta\}\\ \{\phi\}\end{bmatrix} = \begin{bmatrix}\{b^1\}\\ \{b^2\}\\ \{b^3\}\\ \{b^4\}\end{bmatrix}$$

where $[K^{mn}]$ and $[b^m](m = 1, 2)$ are defined as

$$\begin{aligned}
K_{ij}^{11} &= \int_{\eta_e}^{\eta_{e+1}} \psi_i\frac{\mathrm{d}\psi_j}{\mathrm{d}\eta}\,\mathrm{d}\eta,\ K_{ij}^{12} = -\int_{\eta_e}^{\eta_{e+1}} \psi_i\psi_j\,\mathrm{d}\eta,\\
K_{ij}^{13} &= K_{ij}^{14} = K_{ij}^{21} = 0,\\
K_{ij}^{22} &= \int_{\eta_e}^{\eta_{e+1}}\left[-n\left(\overline{h}'\right)^{n-1}\frac{\mathrm{d}\psi_i}{\mathrm{d}\eta}\frac{\mathrm{d}\psi_j}{\mathrm{d}\eta} + \left(\frac{2n}{n+1}\right)\overline{f}\psi_i\frac{\mathrm{d}\psi_j}{\mathrm{d}\eta} - \overline{h}\psi_i\psi_j - M\psi_i\psi_j\right]\mathrm{d}\eta,\\
K_{ij}^{23} &= \Lambda\int_{\eta_e}^{\eta_{e+1}} \psi_i\psi_j\,\mathrm{d}\eta,\ K_{ij}^{24} = N\Lambda\int_{\eta_e}^{\eta_{e+1}} \psi_i\psi_j\,\mathrm{d}\eta,\\
K_{ij}^{31} &= K_{ij}^{32} = 0,\\
K_{ij}^{33} &= \int_{\eta_e}^{\eta_{e+1}}\left[-\frac{1}{Pr}\left(1+\frac{4R_d}{3}\right)\frac{\mathrm{d}\psi_i}{\mathrm{d}\eta}\frac{\mathrm{d}\psi_j}{\mathrm{d}\eta} + \left(\frac{2n}{n+1}\right)\overline{f}\psi_i\frac{\mathrm{d}\psi_j}{\mathrm{d}\eta} + Nb\overline{\phi}'\psi_i\frac{\mathrm{d}\psi_j}{\mathrm{d}\eta} + Nt\overline{\theta}'\psi_i\frac{\mathrm{d}\psi_j}{\mathrm{d}\eta}\right]\mathrm{d}\eta,\\
K_{ij}^{34} &= K_{ij}^{41} = K_{ij}^{42} = 0,\ K_{ij}^{43} = -\frac{Nt}{Nb}\int_{\eta_e}^{\eta_{e+1}}\frac{\mathrm{d}\psi_i}{\mathrm{d}\eta}\frac{\mathrm{d}\psi_j}{\mathrm{d}\eta}\,\mathrm{d}\eta,\\
K_{ij}^{44} &= \int_{\eta_e}^{\eta_{e+1}}\left[-\frac{\mathrm{d}\psi_i}{\mathrm{d}\eta}\frac{\mathrm{d}\psi_j}{\mathrm{d}\eta} + Le\left(\frac{2n}{n+1}\right)\overline{f}\psi_i\frac{\mathrm{d}\psi_j}{\mathrm{d}\eta}\right]\mathrm{d}\eta.
\end{aligned} \tag{30}$$

and

$$\begin{aligned}
b_i^1 &= 0,\ b_i^2 = -\left[\left(\frac{a}{c}\right)^2 + M\left(\frac{a}{c}\right)\right]\int_{\eta_e}^{\eta_{e+1}}\psi_i\,\mathrm{d}\eta - n\left(\overline{h}'\right)^{n-1}\left(\psi_i\frac{\mathrm{d}h}{\mathrm{d}\eta}\right)_{\eta_e}^{\eta_{e+1}},\\
b_i^3 &= -\frac{1}{Pr}\left(1+\frac{4R_d}{3}\right)\left(\psi_i\frac{\mathrm{d}\theta}{\mathrm{d}\eta}\right)_{\eta_e}^{\eta_{e+1}},\ b_i^4 = -\left(\psi_i\frac{\mathrm{d}\phi}{\mathrm{d}\eta}\right)_{\eta_e}^{\eta_{e+1}} - \frac{Nt}{Nb}\left(\psi_i\frac{\mathrm{d}\theta}{\mathrm{d}\eta}\right)_{\eta_e}^{\eta_{e+1}}.
\end{aligned} \tag{31}$$

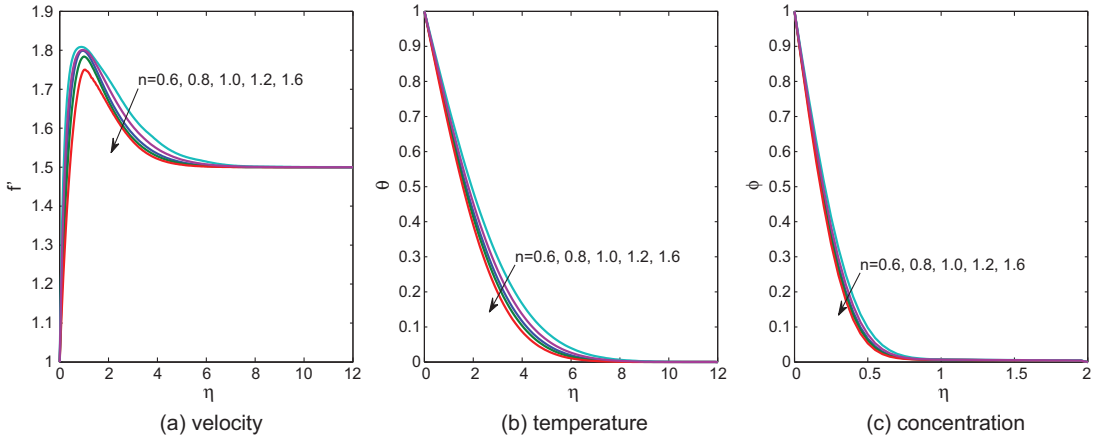

Fig. 1. Effect of power-law index n on velocity, temperature and concentration profiles.

Table 4 Computations of the Nusselt number, skin friction coefficient and the Sherwood number for various values of n and Nb.

n	Nb	$f''(0)$	$-(1+\frac{4R_d}{3})\theta'(0)$	$-\phi'(0)$
0.6	0.2	3.4308	2.0872	2.5483
	0.6	3.4300	2.0219	2.5551
1.0	0.2	2.3758	2.3684	2.8038
	0.6	2.3758	2.3619	2.8114
1.6	0.2	1.4333	2.5683	2.9810
	0.6	1.4333	2.4981	2.9846

where

$$\overline{f}=\sum_{i=1}^{2}\overline{f}_i\psi_i,\ \overline{h}=\sum_{i=1}^{2}\overline{h}_i\psi_i,\ \overline{h'}=\sum_{i=1}^{2}\overline{h}'_i\psi_i,\ \overline{\theta'}=\sum_{i=1}^{2}\overline{\theta}'_i\psi_i,\ \overline{\phi}=\sum_{i=1}^{2}\overline{\phi}'_i\psi_i. \tag{32}$$

Each element matrix is of the order 8×8. The whole domain is divided into 100 linear elements of equal size, after assembly of all the elements equations, we obtain a matrix of the order 404×404. This system of equations as obtained after, assembly of the element equations, is non-linear. Therefore, an iterative scheme must be utilized in the solution. After imposing the boundary conditions only a system of 397 equations remains for the solution, which is solved by the Gauss elimination method maintaining an accuracy of 10^{-4}.

4. Result and discussion

The numerical solutions of governing equations (11)–(13) with boundary conditions (14) have been solved by using the variational finite element method. To validate our results the numerical computations of these skin friction coefficient, Nusselt number and Sherwood number which are respectively, proportional to $f''(0)$, $-(1+\frac{4R_d}{3})\theta'(0)$ and $-\phi'(0)$ are presented in tabular form and one results are compared with Mahapatra [35]. The validation of present results has been verified with the classical case of Newtonian fluid ($n=1$) and there is a good agreement between present and Mahapatra [35] (Table 1).

Table 5 Computations of the Nusselt number, skin friction coefficient and the Sherwood number for various values of Λ, a/c, Le, Pr and Rd.

Λ	a/c	Le	Pr	Rd	$f''(0)$	$-(1+\frac{4R_d}{3})\theta'(0)$	$-\phi'(0)$
–1	1.5	10	0.71	5	0.5400	2.1505	2.5521
0	1.5	10	0.71	5	1.0258	2.2182	2.6209
1	1.5	10	0.71	5	1.4925	2.2776	2.6832
3	1.5	10	0.71	5	2.3873	2.3856	2.7928
3	1.8	10	0.71	5	3.0008	2.5332	2.8682
3	2.0	10	0.71	5	3.4425	2.6278	2.9193
3	1.5	20	0.71	5	1.542	0.9756	1.6267
3	1.5	30	0.71	5	1.0333	0.9756	1.9603
3	1.5	10	1	5	2.3475	2.7862	2.7804
3	1.5	10	10	5	2.0817	7.2348	2.5987
3	1.5	10	100	5	1.8883	10.2348	2.5387
3	1.5	10	0.71	10	2.4258	3.3600	2.8093
3	1.5	10	0.71	15	2.4500	4.1597	2.8163

To analyse the results, numerical computations have been carried out for the dimensionless velocity, temperature and nano partical volume fraction distributions for the flow under considerations and are obtained and their behavior have been discussed for various governing parameters such as magnetic parameter M, dimensionless mixed convection parameter Λ, concentration to thermal buoyancy ratio N, Prandtl number Pr, radiation parameter R_d, Brownian motion Nb, thermophoresis parameter Nt, Lewis number Le. Tables 2, 3, 4, 5 show the effect of magnetic parameter M, power-law index n, dimensionless mixed convection parameter Λ, Prandtl number Pr, radiation parameter R_d, Brownian motion Nb, thermophoresis parameter Nt, Lewis number Le on the coefficient of skin friction coefficient $f''(0)$, Nusselt number $-(1+\frac{4R_d}{3})\theta'(0)$ and Sherwood number $-\phi'(0)$ respectively.It can be seen that the effect of magnetic field parameter M is to decreases the values of $f''(0)$, $-(1+\frac{4R_d}{3})\theta'(0)$ and $-\phi'(0)$. The skin friction coefficient $f''(0)$ decreases with the increase of power-law index n. It is also observed that Nusselt number $-(1+\frac{4R_d}{3})\theta'(0)$ and Sherwood number $-\phi'(0)$ increases with the increase of power-law index n. The skin friction coefficient $f''(0)$ value increases with the increase of thermophoresis parameter Nt. Nusselt number $-(1+\frac{4R_d}{3})\theta'(0)$ and Sherwood number $-\phi'(0)$ decreases with the increase of thermophoresis parameter Nt. The effect of

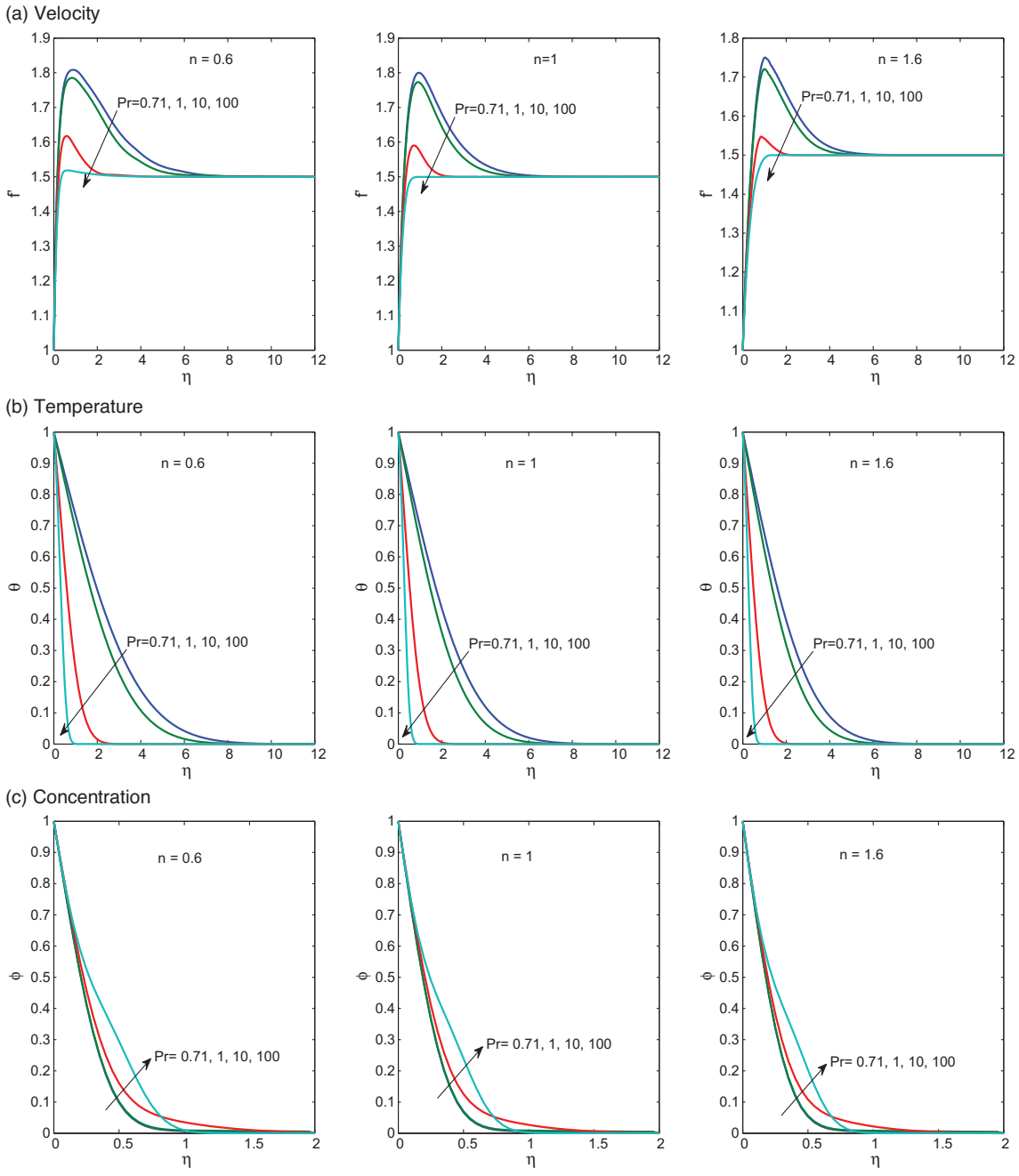

Fig. 2. Effect of *Pr* on velocity, temperature and concentration profiles for pseudo-plastic, Newtonian and dilatant fluids.

Brownian motion parameter *Nb* is to decreases with $f''(0)$ values in case of $n < 1$ and it does not have any effect in case of $n = 1$ and $n > 1$. The effect of Brownian motion parameter (*Nb*) is to decreases the Nusselt number $-(1 + \frac{4R_d}{3})\theta'(0)$ and increases Sherwood number $-\phi'(0)$ for Newtonian and non-Newtonian fluids.

From Table 5 it can be seen that skin friction coefficient $f''(0)$ is to increase with the increase of Λ, a/c and *Rd* whereas skin friction coefficient $f''(0)$ values decreases with the increase of *Le*, *Pr*. The Nusselt number $-(1 + \frac{4R_d}{3})\theta'(0)$ and Sherwood number $-\phi'(0)$ values increases with the increase of Λ, a/c and *Rd*. As *Le* increases Sherwood number $-\phi'(0)$ increases. The effect of Pr is to increases Nusselt number $-(1 + \frac{4R_d}{3})\theta'(0)$ and decreases the Sherwood number $-\phi'(0)$.

Fig. 1(a)–(c) illustrate the variation of velocity, temperature and nanoparticles volume fraction profiles respectively for different values of power-law index *n*. The velocity, temperature and nanoparticles volume fraction profiles decreases with the increase of power-law index *n* from 0.6 to 1.6. The effect of the increases values of *n* is to reduce the boundary layer thickness. It can be observed from Fig. 1(b) effect of power-law index *n* increases from 0.6 to 1.6 the temperature profiles decreases with an increasing viscosity of nanofluid, thermal diffusion is depressed in the resume with cools the boundary layer and

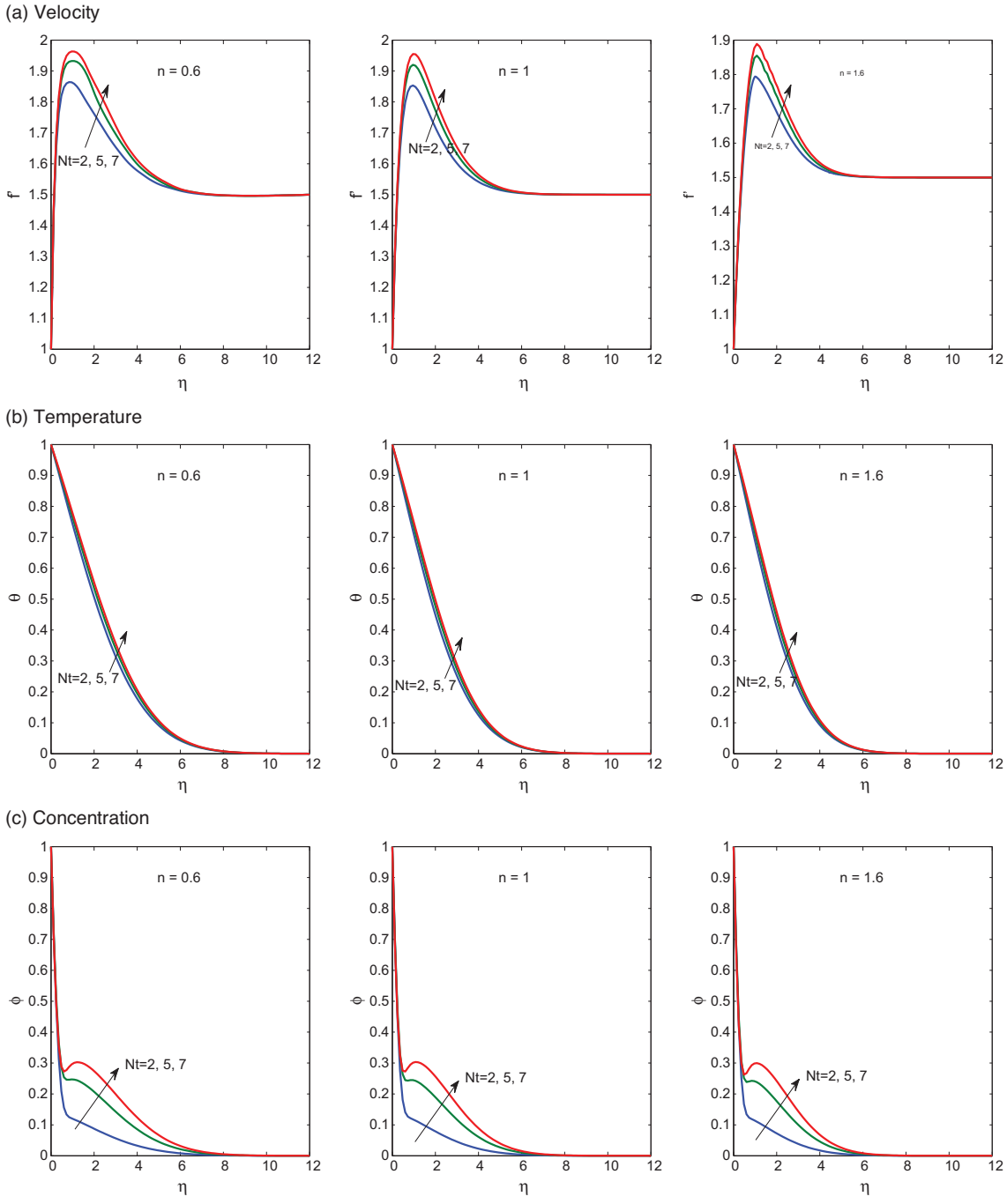

Fig. 3. Effect of *Nt* on velocity, temperature and concentration profiles for pseudo-plastic, Newtonian and dilatant fluids.

decreases the boundary layer thickness. It can also seen from Fig. 1(c) the increase of power-law index n from 0.6 to 1.6 decreases the nanoparticle volume fraction i.e, decreases diffusion of nanoparticle volume fraction (concentration) boundary layer thickness.

Fig. 2(a)–(c) drawn for the velocity, temperature and concentration profiles for different values of Prandtl number Pr for the cases shear-thinning ($n < 1$), Newtonian ($n = 1$) and shear-thickening ($n > 1$) fluids. The effect of Prandtl number Pr is to reduce the velocity and temperature profiles for both Newtonian and non-Newtonian fluids. Physically, fluids with smaller Prandtl number Pr have larger thermal diffusivity. Fig. 2(c) indicated that increasing Prandtl number Pr leads to increase the concentration profile for both Newtonian and non-Newtonian fluids. The effect of thermophoresis parameter Nt is to increase velocity, temperature and concentration profiles for both Newtonian and non-Newtonian fluids is noticed from Fig. 3.

Fig. 4 exhibits dimensionless velocity, temperature and concentration profiles for various values of Brownian motion parameter Nb. It can be seen that the temperature profile slightly increases with an increasing in the value of Brownian motion parameter Nb. The concentration profiles decreases with the value of Brownian motion parameter Nb is noticed from these figure.

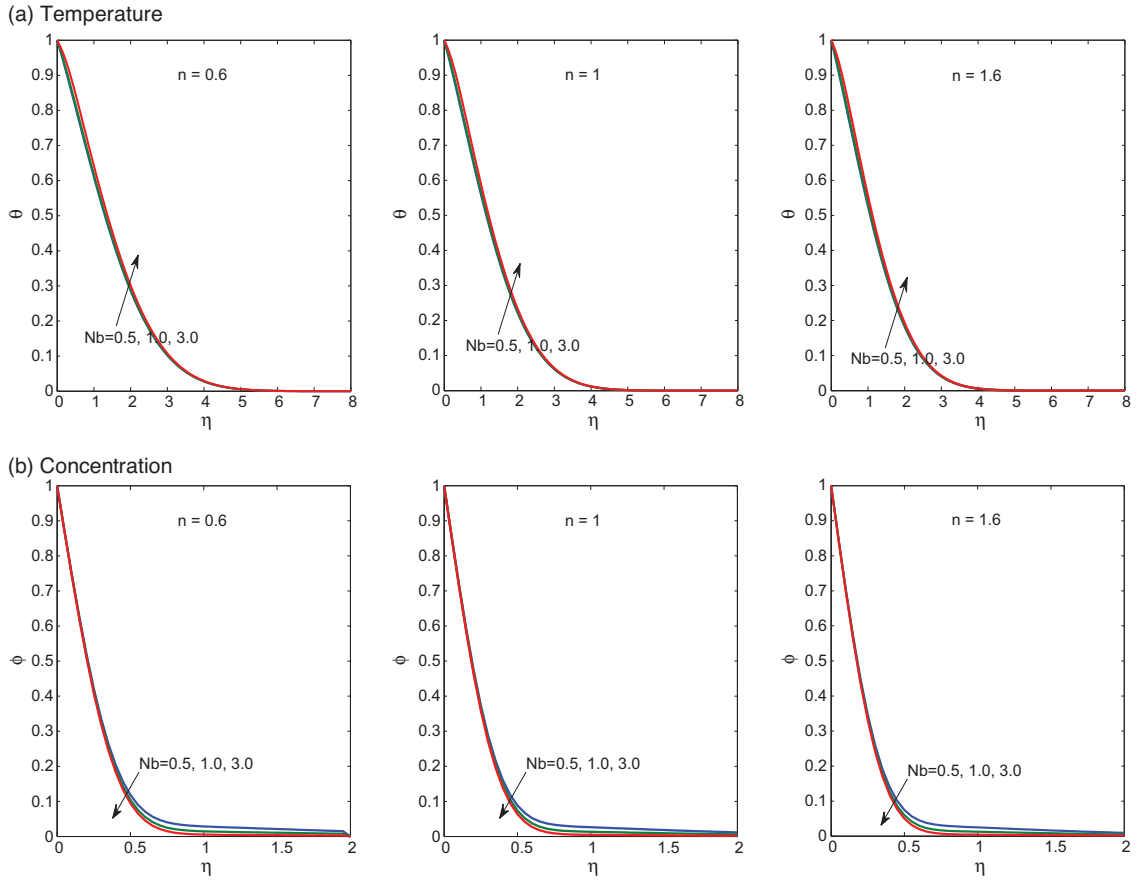

Fig. 4. Effect of *Nb* on temperature and concentration profiles for pseudo-plastic, Newtonian and dilatant fluids.

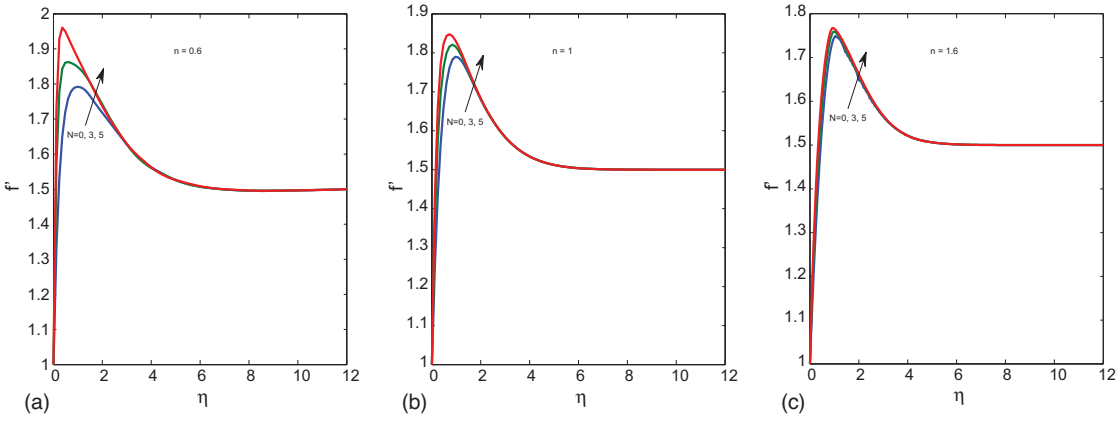

Fig. 5. Effect of *N* on velocity profiles for pseudo-plastic, Newtonian and dilatant fluids.

Fig. 5 shows that the effect of thermal buoyancy ratio N on velocity profiles for shear-thinning ($n < 1$), Newtonian ($n = 1$) and shear-thickening ($n > 1$) fluids respectively. It is noticed that with the increase of N values have a tendency to increase the buoyancy effects changing more induced flow along the stretching sheet in the vertical direction reflected by the increase in the fluid velocity. This enhancement in the fluid velocity has more in shear-thinning fluid ($n < 1$) than shear-thickening fluid ($n > 1$).

Fig. 6(a) shows that the effect of radiation parameter R_d on the velocity profiles for both Newtonian and non-Newtonian fluids. It is noticed from the figure that the velocity of the fluid increases with the increase of radiation parameter R_d values. It can be shown from the Fig. 6(b) that temperature of the fluid increases with the increase of radiation parameter R_d. As expected, an increase of the radiation parameter R_d has the tendency to increase the effect of conduction as well as to increase the temperature at each point away from the surface. Hence, higher values of radiation parameter R_d implies a higher surface heat flux.

Fig. 7(a)–(c) presents the changes in the velocity profiles with the effect of magnetic parameter M for shear-thinning ($n < 1$),

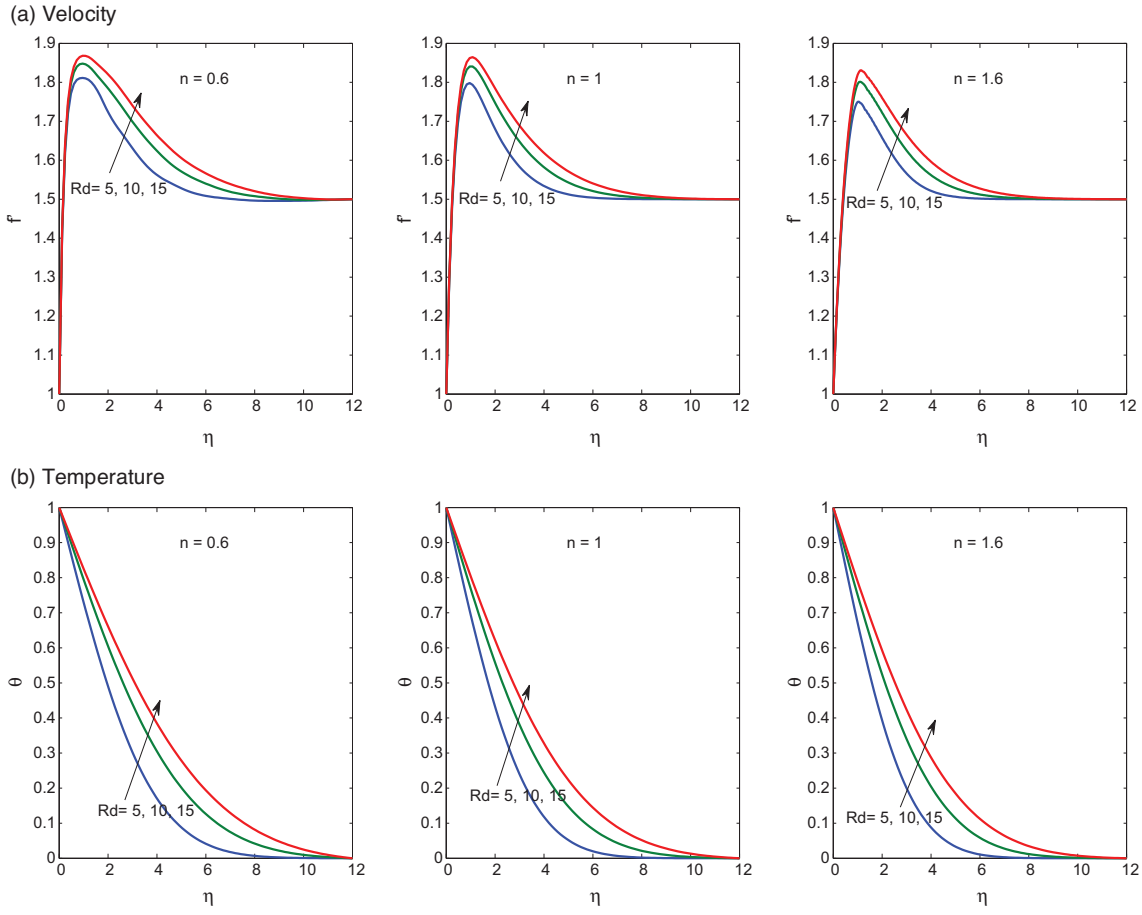

Fig. 6. Effect of *Rd* on velocity and temperature profiles for pseudo-plastic, Newtonian and dilatant fluids.

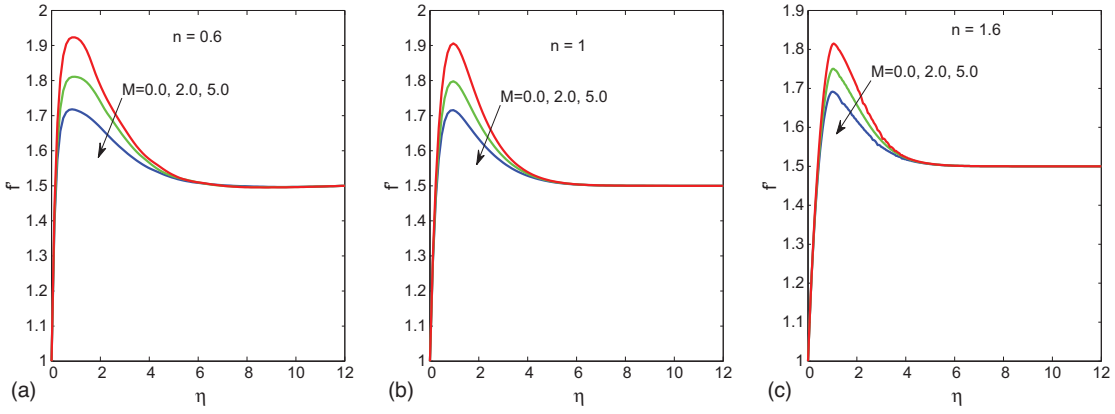

Fig. 7. Effect of *M* on velocity profiles for pseudo-plastic, Newtonian and dilatant fluids.

Newtonian ($n = 1$) and shear-thickening ($n > 1$) fluids respectively. The velocity profiles f' decreases with the raising of magnetic parameter M. This is due to magnetic field opposing the transport phenomena, since the variation of magnetic parameter M causes the variation of Lorentz forces. The Lorentz force is a drag-like force that produces more resistance to transport phenomena and that causes reduction in the fluid velocity. The effect of magnetic field is more in shear thinning fluids than shear thickening fluids. The effect of magnetic fields is very meager on temperature profiles hence it is not shown.

Fig. 8(a)–(c) shows that the effect of dimensionless mixed convection parameter Λ on velocity, temperature and concentration profiles respectively. The velocity profiles are increasing with increasing values of Λ whereas temperature and concentration profiles are decreasing with increasing values of Λ. The presence of the thermal buoyancy effects represented by finite

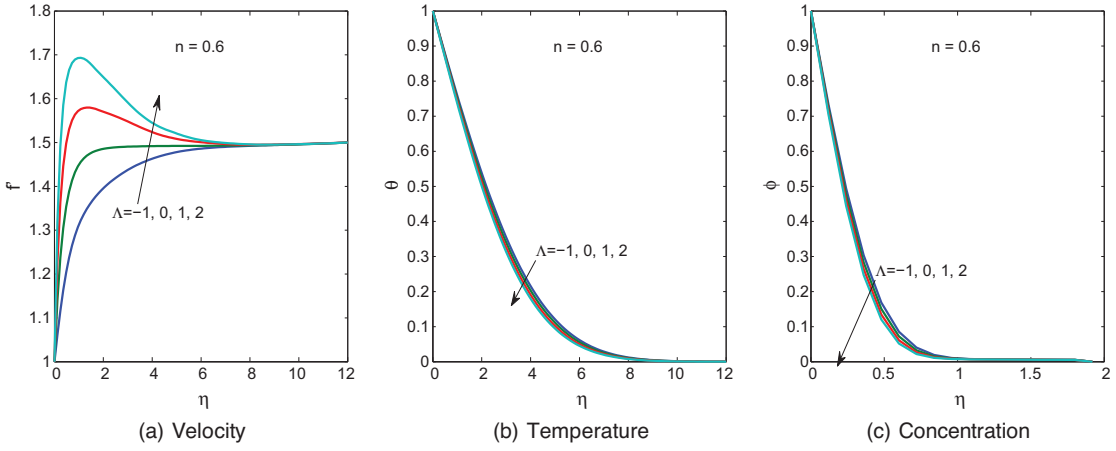

Fig. 8. Effect of Λ on the velocity, temperature and concentration profiles for $n = 0.6$.

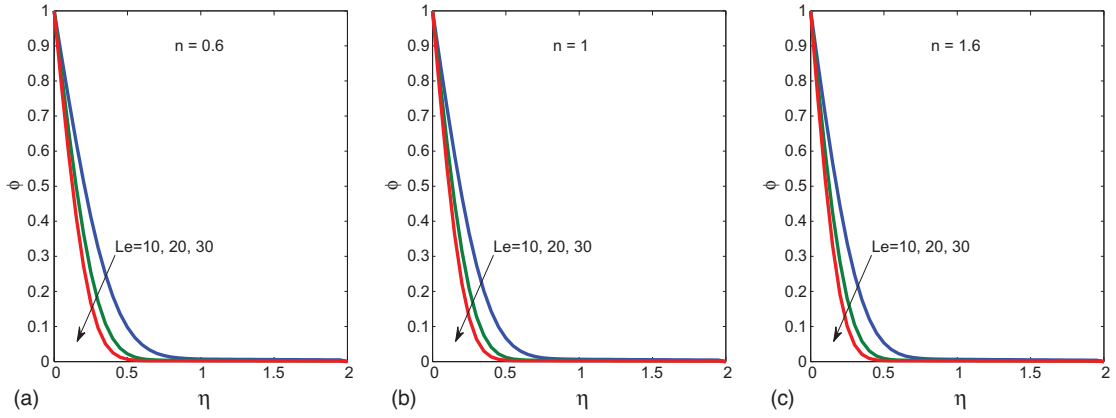

Fig. 9. Effect of *Le* on concentration profiles for pseudo-plastic, Newtonian and dilatant fluids.

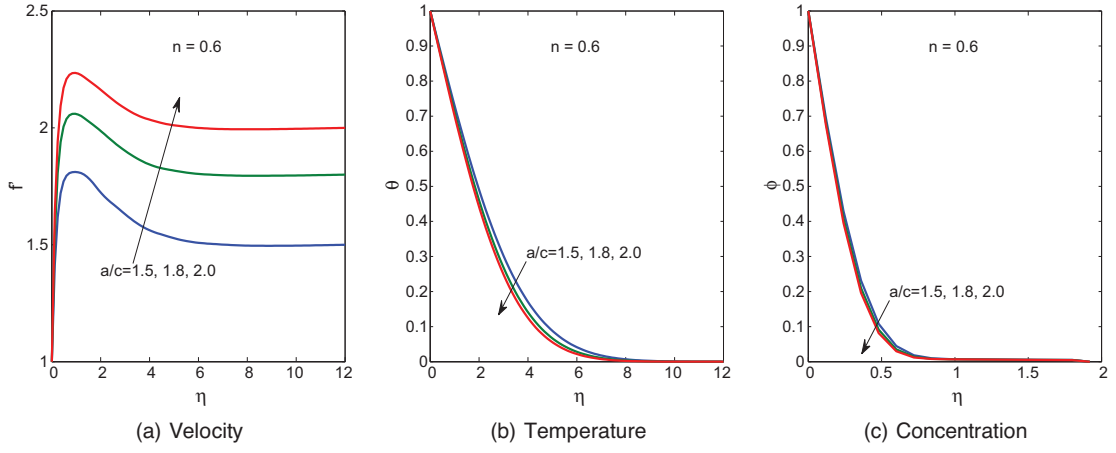

Fig. 10. Effect of a/c on the velocity, temperature and concentration profiles for $n = 0.6$.

values of the mixed parameter has the tendency to induce more flow along the surface at the expense of small reductions in the temperature and concentration. Distinctive peaks in the velocity profiles which are characteristics of free-convection flows are also observed as Λ increases.

Fig. 9 shows the variation of nanoparticle concentration profiles for Newtonian and non-Newtonian fluids with different values of Lewis number *Le*. The concentration profile is decreased due to increase of Lewis number *Le*. Increasing in the Lewis number *Le* reduces the nanoparticle volume fraction and its boundary layer thickness.

Fig. 10(a)–(c) present the velocity, temperature and concentration profiles for various values of ratio of velocity parameter a/c. It can be observed that an increase in a/c causes increase

in velocity profiles and significant decrease on the temperature and concentration profiles. These behaviors are clearly shown in Fig. 10.

5. Conclusions

The influence of Brownian motion and thermophoresis on mixed convection magneto hydrodynamic boundary layer flow of heat and mass transfer stagnation point flow of power-law non-Newtonian nanofluid towards a stretching surface is investigated. The main findings of the present study can be summarised as follows:

- The effect of magnetic field parameter M reduces the velocity profiles.
- The influence of thermophoresis parameter Nt is to increase the velocity, temperature and concentration profiles for both newtonian and non-Newtonian fluids. The effect of Brownian motion Nb is to increases the temperature profiles and decreases the concentration profiles.
- The velocity and concentration profiles are increases with the increase of radiation parameter R_d for both newtonian and non-Newtonian fluids.
- With the effect of mixed convection parameter Λ and velocity ratio parameter a/c are to increase the velocity profiles and reduces the temperature and concentration profiles.
- The skin friction co-efficient $f''(0)$ increases with the increase of thermophoresis parameter Nt and it decreases with the increase of Brownian motion parameter Nb and the power-law index n. The co-efficient of nusslet number and sherwood number decreases with the increase of Nt.

Acknowledgment

Authors are grateful to the reviewers for their comments and suggestions which helped them to improve the quality of the research paper.

References

[1] W.R. Schowalter, The application of boundary layer theory to power-law pseudoplastic fluid: similar solutions, AIChE J. 6 (2004) 24–28.
[2] A. Acrivos, On laminar boundary layer flows with a rapid homogeneous chemical reaction, Chem. Eng. Sci. 13 (1960) 57–62.
[3] E.M.A. Elbashbeshy, T.G. Emam, M.S. Abdel-wahed, Three - dimensional flow over a stretching surface with thermal radiation and heat generation in the presence of chemical reaction and suction/injection, Int. J. Energy Technol. 16 (2011) 1–8.
[4] S. Nadeem, T. Hayat, M.Y. Malik, S.A. Rajput, Thermal radiations effects on the flow by an exponentially stretching surface: a series solution, Z. Naturforschung 65 (2010) 1–9.
[5] S. Nadeem, A. Hussain, K. Vajravelu, Effects of heat transfer on the stagnation flow of a third order fluid over a shrinking sheet, Z. Naturforschung A 65 (2010) 969–994.
[6] S. Nadeem, A. Hussain, M. Khan, Ham solutions for boundary layer flow in the region of the stagnation point towards a stretching sheet, Commun. Nonlinear Sci. Numer. Simul. 15 (2010) 475–481.
[7] S. Nadeem, N.S. Akbar, Influence of heat transfer on a peristaltic flow of johnson segalman fluid in a non-uniform tube, Int. Commun. Heat Mass Transf. 36 (2009) 1050–1059.
[8] S. Nadeem, M. Ali, Analytical solutions for pipe flow of a fourth grade fluid with reynolds and vogel's models of viscosities, Commun. Nonlinear Sci. Numer. Simul. 14 (2009) 2073–2090.
[9] J. Buongiorno, Convective transport in nanofluids, ASME J. Heat Transf. 128 (2006) 240–250.
[10] G. Lukaszewicz, Asymptotic behavior of micropolar fluid flows, Int. J. Eng. Sci. 41 (2003) 259–269.
[11] A.V. Shenoy, non-newtonian fluid heat transfer in porous media, Adv. Heat Transf. 24 (1994) 101–190.
[12] G. Astarita, G. Marrucci, Principles of NonNewtonian Fluid Mechanics, McGraw-Hill, New York, 1974.
[13] H. Bohme, Nonnewtonian fluid mechanics,northholland series in applied mathematics and mechanics, North-Holland, 1987.
[14] N. Kishan, B.S. Reddy, Mhd effects on non-newtonian power-law fluid past a continuously moving porous flat plate with heat flux and viscous dissippation, Int. J. Appl. Mech. Eng. 18 (2013) 425–445.
[15] P. Kavitha, N. Kishan, Mhd flow of a non-newtonian power-law fluid over a stretching sheet with thermal radiation, viscous dissipation and slip boundary conditions, Acta Tech. 59 (2014) 355–376.
[16] S. Nadeem, A. Riaz, R. Ellahi, N.S. Akbar, Effects of heat and mass transfer on peristaltic flow of a nanofluid between eccentric cylinders, Appl Nanosci. 4 (2013) 393–404.
[17] D.W. Zhou, Heat transfer enhancement of copper nanofluid with acoustic cavitation, Int. J. Heat Mass Transf. 47 (2004) 3109–3117.
[18] S.U.S. Choi, Enhancing thermal conductivity of fluids with nanoparticle, ASME Fluids Eng. Div. 231 (1995) 99–105.
[19] Y. Xuan, Q. Li, Investigation on convective heat transfer and flow features of nanofluids, J. Heat Transf. 125 (2003) 151–155.
[20] Pak, Cho, Hydrodynamic and heat transfer study of dispersed fluids with submicron metallic oxide particles, Exp. Heat Transf. 11 (1998) 150–170.
[21] D.S. Wen, Y.L. Ding, Effective thermal conductivity of aqueous suspensions of carbon nanotubes (nanofluids), J. Thermophys. Heat Transf. 18 (2004) 481–485.
[22] Y.L. Ding, H. Alias, D.S. Wen, R.A. Williams, Heat transfer of aqueous suspensions of carbon nanotubes (cnt nanofluids), Int. J. Heat Mass Transf. 49 (2006) 240–250.
[23] H. Masuda, A. Ebata, K. Teramae, N. Hishiunma, Alteration of thermal conductivity and viscosity of liquid by dispersed ultra-fine particles, Dispersion of -$Al_2O_3SiO_2$ and TiO_2 ultra-fine particles, Netsu Bussei (Japan) 4 (1993) 227–233.
[24] P. Keblinski, S.R.E. Phillpot, S.U.S. Choi, J.A. Eastman, Mechanisms of heat flow in suspensions of nano-sized particles (nanofluids), Int. J. Heat Mass Transf. 45 (2002) 855–863.
[25] D.T. Wasan, A.D. Nikolov, Spreading of nanofluids on solids, Nature 423 (2003) 156–159.
[26] A. Chengara, A.D. Nikolov, D.T. Wasan, A. Trokhymchuk, D. Henderson, Spreading of nanofluids driven by the structural disjoining pressure gradient, J. Colloid Interface Sci. 280 (2004) 192–201.
[27] S.M. You, J.H. Kim, K.H. Kim, Effect of nanoparticles on critical heat flux of water in pool boiling heat transfer, Appl. Phys. Lett. 83 (2003) 3374–3376.
[28] M. Sheikholeslami, R. Ellahi, H.R. Ashorynejad, G. Domairry, T. Hayat, Effects of heat transfer in flow of nanofluids over a permeable stretching wall in a porous medium, Comput. Theor. Nanosci. 11 (2014) 486–496.
[29] L.J. Crane, Flow past a stretching plate, Z. Angew. Math. Phys. 21 (1970) 645–655.
[30] P. Carragher, L.J. Crane, H.t. o. a. c. s. sheet, Z. Angew. Math. Mech. 62 (1982) 564–573.
[31] R. Ellahi, M. Raza, K. Vafai, Series solutions of non-newtonian nanofluids with reynolds model and vogels model by means of the homotopy analysis method, Math. Comput. Model. 55 (2012) 1876–1891.
[32] R. Ellahi, S. Aziz, A. Zeeshan, Non newtonian nanofluids flow through a porous medium between two coaxial cylinders with heat transfer and variable viscosity, J. Porous Media 16 (2013) 205–216.

[33] R. Ellahi, The effects of mhd and temperature dependent viscosity on the flow of non-newtonian nanofluid in a pipe: analytical solutions, Appl. Math. Model. 37 (2013) 1451–1457.
[34] K.V. Prasad, K. Vajravelu, P.S. Datti, Mixed convection heat transfer over an on-linear stretching surface with variable fluid properties, Int. J. Non-Linear Mech. 45 (2010) 320–330.
[35] T.R. Mahapatra, S.K. Nandy, A.S. Gupta, Analytical solution of magnetohydrodynamic stagnation-point flow of a power-law fluid towards a stretching surface, Appl. Math. Comput. 215 (2009) 1696–1710.